absorption bands ($\lambda_{max} = 535$ nm for **1b** and $\lambda_{max} = 630$ nm for **2b**) correspond to the long-axis electronic transition of the closed-ring isomers (see Scheme 1). The absorption anisotropy of **2b** in the crystal **1a**/**2a** was similar to that of **1b**. This indicates that **2a** is packed in a similar manner as **1a** in the crystal **1a**/**2a**, and both components undergo photochromic reactions in the crystal lattice. The long-axis electronic transition moments of the photogenerated closed-ring isomers **1b** and **2b** are parallel to each other.

The absorption spectral change was further demonstrated by taking a photograph of the irradiated crystal. By recrystallization of a mixture of **1a** and **2a** (95:5) from ethanol, a two-component crystal **1a**/**2a** was obtained, whose composition ratio was 99.6:0.4 as determined by HPLC. Figure 4 shows a

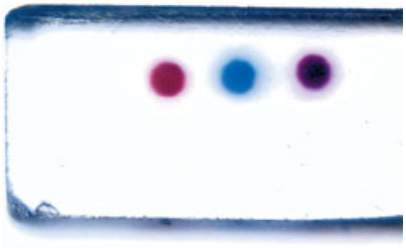

Fig. 4. Photograph of partially colored crystal **1a**/**2a**. Left: irradiated with 370 nm light. Middle: irradiated with 405 nm light. Right: irradiated with both 370 nm and 405 nm light.

photograph of the partially colored surface A of the crystal. The colorless crystal turned red upon irradiation with 370 nm light, and turned blue by 405 nm light. Upon irradiation with both 370 nm and 405 nm light, it turned purple. We can regard each colored spot as a bit in optical recording media. By changing the wavelength of irradiating light (370 nm and 405 nm light), four kinds of information, such as colorless, red, blue, and purple, could be written into the crystal. The recording density of the two-wavelength recording using the two-component photochromic crystal is twice as large as for common one-component crystal systems.

In summary, we prepared photochromic single crystals of a diarylethene mixture composed of **1a** and **2a**. By changing the wavelength of irradiating light, the two components selectively underwent photochromic reactions in the single crystals. The colorless crystals turned red, blue, or purple. Such multicolored photochromic crystals have potential for the application to high-density memories and multi-color displays.

## *Experimental*

Solvents used were spectroscopic grade and purified by distillation before use. Absorption spectra in a single-crystalline phase were measured using a Leica DMLP polarizing microscope connected with a Hamamatsu PMA-11 photodetector. Polarizer and analyzer were set in parallel to each other. Photoirradiation was carried out using a 75 W xenon lamp. The wavelength of the light used for the photocyclization and photocycloreversion reactions was selected by passing the light through a band pass filter. The selected wavelengths were 370 nm ($\Delta\lambda_{1/2} = 20$ nm) and 405 nm ($\Delta\lambda_{1/2} = 17$ nm) for the cyclization reactions, and 492 nm ($\Delta\lambda_{1/2} = 14$ nm) and 692 nm ($\Delta\lambda_{1/2} = 16$ nm) for the cycloreversion reactions. X-ray crystallographic analysis was carried out using a Bruker SMART CCD X-ray diffractometer. The composition ratio of **1a** and **2a** in crystal **1a**/**2a** was measured by a HPLC equipped with a silica gel column (Wako, Wakosil 5SIL) using hexane/ethyl acetate (95:5) as the eluent.

Received: March 11, 2002
Final version: April 25, 2002

[1] G. H. Brown, *Photochromism*, Wiley-Interscience, New York **1971**.
[2] H. Dürr, H. Bouas-Laurent, *Photochromism: Molecules and Systems*, Elsevier, Amsterdam **1990**.
[3] V. Ramamurthy, K. Venkatesan, *Chem. Rev.* **1987**, *87*, 433.
[4] J. R. Scheffer, P. R. Pokkuluri, in *Photochemistry in Organized & Constrained Media* (Eds: V. Ramamurthy), VCH, New York **1990**, p. 185.
[5] J. H. Golden, *J. Chem. Soc.* **1961**, 3741.
[6] a) K. Maeda, T. Hayashi, *Bull. Chem. Soc. Jpn.* **1970**, *43*, 429. b) M. Kawano, T. Sano, J. Abe, Y. Ohashi, *J. Am. Chem. Soc.* **1999**, *121*, 8106. c) M. Kawano, T. Sano, J. Abe, Y. Ohashi, *Chem. Lett.* **2000**, 1372.
[7] K. Ichimura, S. Watanabe, *Bull. Chem. Soc. Jpn.* **1976**, *49*, 2220.
[8] A. M. Trozzolo, T. M. Leslie, A. S. Sarpotdar, R. D. Small, G. J. Ferraudi, T. DoMinh, R. L. Hartless, *Pure Appl. Chem.* **1979**, *51*, 261.
[9] a) H. Sixl, R. Warta, *Chem. Phys.* **1985**, *94*, 147. b) Y. Eichen, J.-M. Lehn, M. Scherl, D. Haarer, J. Fischer, A. DeCian, A. Corval, H. P. Trommsdorff, *Angew. Chem. Int. Ed. Engl.* **1995**, *34*, 2530. c) J. Takeda, S. Shinohara, N. Eguchi, S. Ohishi, S. Kurita, T. Kodaira, *J. Phys. Soc. Jpn.* **1999**, *68*, 1423. d) A. Schmidt, S. Kababya, M. Appel, S. Khatib, M. Botoshansky, Y. Eichen, *J. Am. Chem. Soc.* **1999**, *121*, 11 291.
[10] a) E. Hadjoudis, M. Vittorakis, I. Moustakali-Mavridis, *Tetrahedron* **1987**, *43*, 1345. b) T. Kawato, H. Koyama, H. Kanatomi, M. Isshiki, *J. Photochem.* **1985**, *28*, 103. c) J. Harada, H. Uekusa, Y. Ohashi, *J. Am. Chem. Soc.* **1999**, *121*, 5809.
[11] Y. Mori, Y. Ohashi, K. Maeda, *Bull. Chem. Soc. Jpn.* **1989**, *62*, 3171.
[12] M. Irie, *Chem. Rev.* **2000**, *100*, 1685.
[13] M. Irie, K. Uchida, T. Eriguchi, H. Tsuzuki, *Chem. Lett.* **1995**, 899.
[14] M. Irie, K. Uchida, *Bull Chem. Soc. Jpn.* **1998**, *71*, 985.
[15] S. Kobatake, T. Yamada, K. Uchida, N. Kato, M. Irie, *J. Am. Chem. Soc.* **1999**, *121*, 2380.
[16] S. Kobatake, M. Yamada, T. Yamada, M. Irie, *J. Am. Chem. Soc.* **1999**, *121*, 8450.
[17] a) T. Kodani, K. Matsuda, T. Yamada, M. Irie, *Chem. Lett.* **1999**, 1003. b) T. Kodani, K. Matsuda, T. Yamada, S. Kobatake, M. Irie, *J. Am. Chem. Soc.* **2000**, *122*, 9631.
[18] T. Yamada, S. Kobatake, K. Muto, M. Irie, *J. Am. Chem. Soc.* **2000**, *122*, 1589.
[19] M. Irie, T. Lifka, S. Kobatake, N. Kato, *J. Am. Chem. Soc.* **2000**, *122*, 4871.
[20] T. Yamada, S. Kobatake, M. Irie, *Bull. Chem. Soc. Jpn.* **2000**, *73*, 2179.
[21] S. Kobatake, K. Shibata, K. Uchida, M. Irie, *J. Am. Chem. Soc.* **2000**, *122*, 12 135.
[22] M. Irie, S. Kobatake, M. Horichi, *Science* **2001**, *291*, 1769.
[23] T. Fukaminato, S. Kobatake, T. Kawai, M. Irie, *Proc. Jpn. Acad., Ser. B* **2001**, *77*, 30.
[24] T. Yamada, K. Muto, S. Kobatake, M. Irie, *J. Org. Chem.* **2001**, *66*, 6164.
[25] K. Shibata, K. Muto, S. Kobatake, M. Irie, *J. Phys. Chem. A* **2002**, *106*, 209.
[26] T. Yamada, S. Kobatake, M. Irie, *Bull. Chem. Soc. Jpn.* **2002**, *75*, 167.
[27] W. J. Tomlinson, E. A. Chandross, R. L. Fork, C. A. Pryde, A. A. Lamola, *Appl. Opt.* **1972**, *11*, 533.
[28] M. Irie, *Photo-Reactive Materials for Ultrahigh-Density Optical Memories*, Elsevier, Amsterdam **1994**.
[29] D. Psaltis, F. Mok, *Sci. Am.* **1995**, *273(5)*, 52.
[30] S. Kawata, Y. Kawata, *Chem. Rev.* **2000**, *100*, 1777.
[31] A. Fernandez-Asebes, J.-M. Lehn, *Adv. Mater.* **1999**, *11*, 910.

## Junctions and Networks of SnO Nanoribbons

By *Zhong Lin Wang** and *Zhengwei Pan*

Research in nanowire materials has attracted a great deal of attention because these quasi-one-dimensional nanomaterials are abundant and of potential technological importance, especially for nanoelectronics and optoelectronics.[1–4] A wide

[*] Prof. Z. L. Wang, Dr. Z. W. Pan
School of Materials Science Engineering, Georgia Institute of Technology
Atlanta, GA 30332-0245 (USA)
E-mail: zhong.wang@mse.gatech.edu

  0935-9648/02/1508-1029 $ 17.50+.50/0 

ADVANCED MATERIALS

range of materials, including metals,[5] semiconductors,[6–8] oxides,[9,10] and polymers,[11,12] have been made into wire shape, with a dimension of a few nanometers to a few tens of nanometers in diameter. Among these materials, semiconducting transparent oxides form a unique group that has important applications in functional and smart devices,[13] such as chemical and biological sensors. The electrical conductivity of these oxides depends sensitively on the type and concentration of molecules adsorbed on their surfaces. The oxides have two important characteristics: 1) cations with mixed valences and 2) significant oxygen vacancies, resulting in a large tunability of their structures and properties.[14]

Quasi-one-dimensional nanobelts and nanowires of ZnO, $SnO_2$, $Ga_2O_3$, $In_2O_3$, CdO, and $PbO_2$ materials for sensor and fuel cell applications have been synthesized.[15–17] The nanobelts have a rectangular cross section and remain uniform along the entire length without a change in width or thickness. Our recent study indicates that the Sn–O nanostructures are rich in both composition and morphology. Using a Sn/SnO mixture as the source material, $SnO_2$ nanoribbons have been synthesized, which have been found to have an orthorhombic structure that is stable and can exist in bulk only if the external pressure is > 150 kbar.[18]

In this paper we report, for the first time, the aligned junctions and networks of SnO nanostructures. These structures have multi-outlets and are ideal objects for the fabrication of nanoscale functional devices.

The as-synthesized samples can have several morphologies: coin-shaped diskettes, nanobelts, square-based columns, and aligned junctions of nanoribbons. The former three will be described in details elsewhere,[19] and we focus on the junctions here. Figure 1a shows a typical SEM image of the junctions and networks of SnO nanoribbons, and a magnified SEM image is given in Figure 1b. The nanoribbons are rather straight and form a crossed network. The tip of a nanoribbon has a large head, which is identified as a Sn metal particle that served as the catalyst for the growth. It is clear that the nanoribbons grow along two specific directions and the network is quite regular.

TEM images of the junctions and networks are given in Figures 2a and b. It is apparent that the Sn nanoparticles are located at or close to the tips of the growth branches, and some of the Sn particles are deposited on the branches. The branches grow orthogonally along either [100] or [010], forming the crossed network. The crystallography of the as-synthesized sample was determined by electron diffraction. Two methods have been used. The first method was based on the real space lattice fringes observed through high-resolution TEM lattice imaging, and the second technique relies on the measurement of lattice constants based on camera length. Since $SnO_2$ has the rutile structure with lattice constants $a = 0.4732$ nm and $c = 0.3184$ nm, and SnO has a tetragonal structure with lattice constants of $a = 0.3802$ nm, $c = 0.4836$ nm, it is easy to distinguish SnO from $SnO_2$ from the [001] and the [012] (Figs. 2c and d) diffraction patterns. Our results show that the junction network has the SnO structure. Chemical analysis using energy dispersive X-ray spectroscopy (EDS) indicates the exclusive presence of Sn and O in the sample.

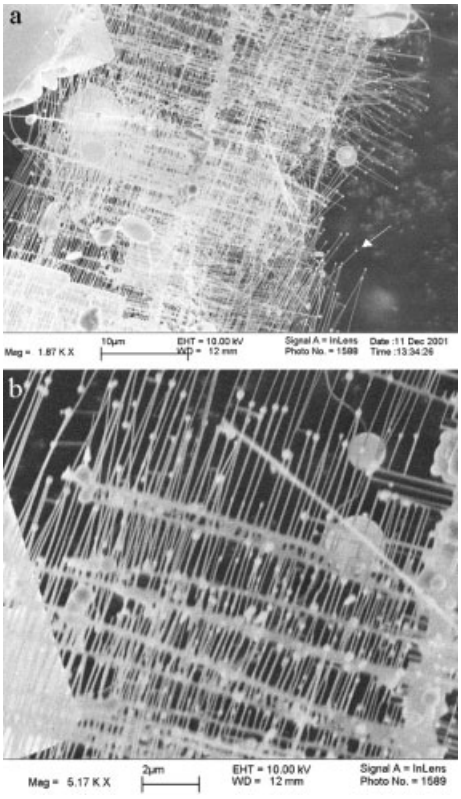


Fig. 1. SEM images of the as-synthesized junction networks of SnO nanoribbons, showing the orthogonal growth of the branches.

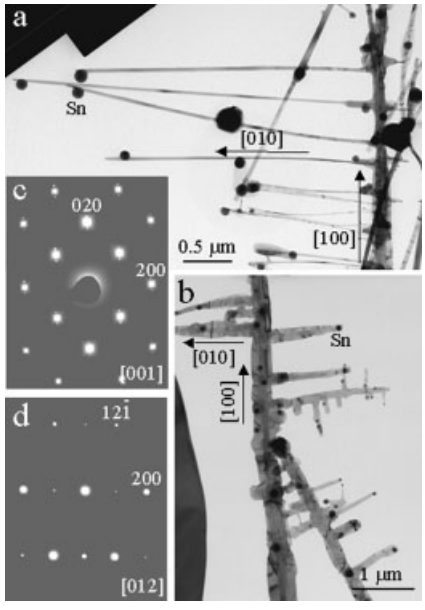


Fig. 2. a,b) TEM images of the junction structures of SnO nanoribbons. c,d) Electron diffraction patterns recorded from nanoribbons to determine its tetragonal structure. The superlattice reflection spots observed in (c) are due to superstructures possibly as a result of ordered oxygen vacancies.

From the SEM images shown in Figure 1, it may be assumed that the networks form a planar structure because the

  0935-9648/02/1508-1030 $ 17.50+.50/0 

growth directions are specific. This anticipated result is confirmed by the TEM image and the corresponding electron diffraction pattern given in Figure 3. The electron diffraction pattern recorded from the ladder region clearly indicates that the branches have the same orientation and they are a single crystal.

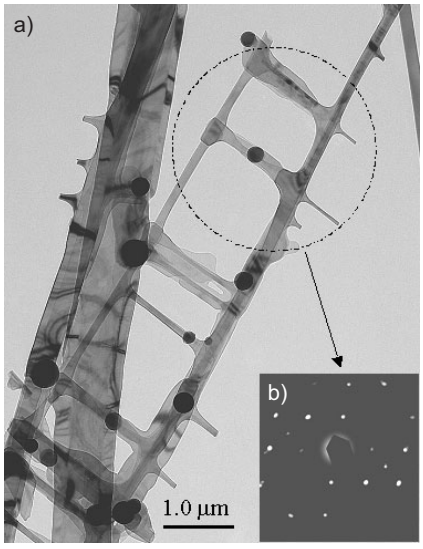


Fig. 3. TEM image of the T- and π-junctions of SnO nanoribbons (a), and the corresponding electron diffraction pattern (b) recorded from the "ladder" structure, showing that the branches are the same crystalline piece.

Figure 4 shows a high-resolution TEM image recorded near the side-edge of the nanoribbon. It is apparent that the nanoribbon grows along the [100] direction. Compared to the background contrast contributed by the amorphous carbon that is used as the substrate for TEM imaging, the (010) side surface is not very flat, at least at the atomic level.

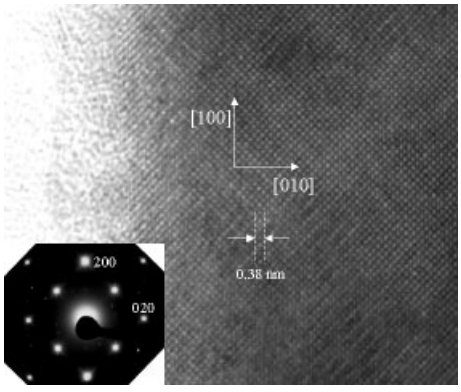


Fig. 4. High-resolution TEM image from a nanoribbon, showing its crystal structure and growth direction. The inset is the corresponding electron diffraction pattern.

The growth of the network is rather unique. Figure 5 shows an SEM image that displays the general morphology of the network. It appears that the network is defined by the aligned SnO nanoribbons, and several typical configurations have been observed. The tips of the nanoribbons are decorated with Sn particles (arrow 1); two nanoribbons can join into one

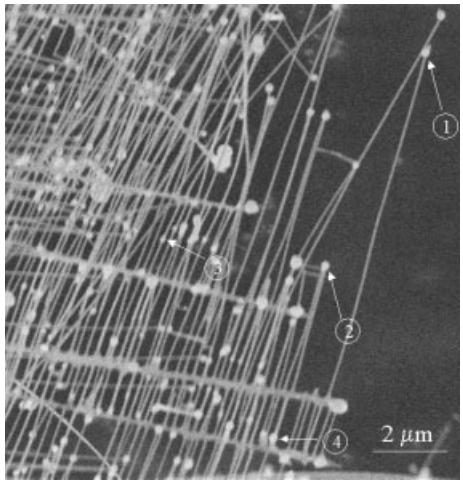


Fig. 5. SEM image of the as-synthesized junction networks of SnO nanoribbons, showing several growth features of the branches.

branch at the tips (arrow 2); the Sn particle can locate at either the middle of the nanoribbon connecting the two main branches (arrow 3) or at the end touching the other branch (arrow 4). Due to the tetragonal structure of SnO, [100] and [010] are equivalent directions, but not [001], therefore, the nanoribbons grow along either the *a*- or *b*-axis, resulting in aligned and crossed planar nanoribbon networks.

From the experimental results demonstrated above, the formation of the Sn metallic particles likely resulted from the following process, which is possible at high temperature:

$$2SnO \rightarrow 2Sn + O_2 \quad (1)$$

It is believed that the Sn metallic particles are produced at the same time the SnO ribbons are formed because the Sn particles are the catalyst for the growth following a vapor–liquid–solid (VLS) mechanism. The Sn particles are liquid droplets at the growth temperature due to their low melting point (232 °C), and serve as the sites for adsorption of SnO vapor. As the main branches grow along [100] with Sn particles at the tip (Fig. 6a), smaller droplets of Sn can be formed on the SnO nanoribbon surface, which leads to the growth of SnO branches along [010], resulting in the formation of the perpendicular branches (Fig. 6b). All of the grown branches are likely to be confined in the (110) plane because the entire piece is a single crystalline structure although strain-induced twisting

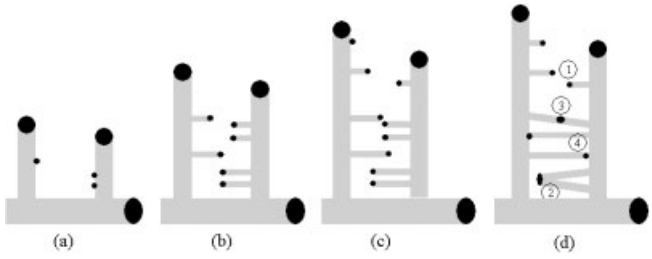


Fig. 6. A proposed model for describing the growth process of the junction networks. For simplicity, the branches grown inwards are shown and those grown outwards are omitted from the diagram.

  0935-9648/02/1508-1031 $ 17.50+.50/0 

ADVANCED MATERIALS

and bending can exist in the nanoribbons. As the side branches grow longer and longer, the branches that cannot meet remain as individual nanoribbons with the Sn particle at the ends (area 1 in Fig. 6d). If two branches are fairly close and continuous growth results in long length nanoribbons with high lateral bending flexibility, the liquid droplets at the tips may recombine when the two tips meet, resulting in joined growth (area 2 in Fig. 6d), as observed in Figure 5 (arrow 2). If two nanoribbons grow next to each other and are located fairly close, they may combine the liquid droplets at the tips into one liquid droplet to reduce the surface energy (area 3 in Fig. 6d, and arrow 3 in Fig. 5). If there is no interruption during the growth, the branch continues to grow until it meets the next nanoribbon (area 4 in Fig. 6d); thus, the growth is terminated and the Sn droplet remains at the cross point.

Considering the low melting point of Sn, the Sn droplets are still liquid while the sample is cooled to below the growth temperature. It is possible that the Sn droplets can slip off the tip and hang on the side of the branch, as observed in the TEM image shown in Figure 2a.

In the literature, a "fishbone" structure of MgO[20] has been reported. The MgO fishbone structure was grown by Co catalyst assisted growth, and the growth was attributed to the VLS process. The semiconducting SnO junctions and networks reported here are intrinsically semiconducting, with controlled structure and orientation. They may have important applications in the fabrication of optoelectronics devices and nanosensors.

## *Experimental*

The experimental set-up used for the synthesis consists of a horizontal tube furnace, an alumina tube, a rotary pump system, and a gas supply and control system. Commercial (Alfa Aesar) SnO powder with a purity of 99.9 % (metals basis) was used as the source material that was placed in an alumina crucible, and the crucible was located at the center of the alumina tube. Several alumina strip plates ($60 \times 10$ mm$^2$) were placed downstream one-by-one inside the alumina tube, which acted as substrates for collecting growth products. After evacuating the alumina tube to $\sim 2 \times 10^{-3}$ torr, thermal evaporation was conducted at 1050–1100 °C for 2 h under 300–400 torr of Ar gas at a flow rate of 50 sccm. The process of material growth inside the alumina tube was monitored in-situ through a quartz window installed at the gas inlet end of the alumina tube during the evaporation.

The SnO network was usually formed at the low-temperature part of the furnace (200–500 °C). Although other kinds of morphologies, such as nanobelts and diskettes, were also formed in this region, the network was mainly present at the top layer of the deposited sample and it can be easily distinguished by color. The network appears as a gold-like color, while the SnO nanobelts are white and SnO diskettes are light brown. It is thus not difficult to separate it from others. The formation and quantity of the network is sensitive to the experimental parameters. For example, the higher the temperature (from 1500 to 1100 °C) and/or the higher the pressure inside the alumina tube (from 300 to 400 torr), the more the network was produced. Under a specific synthesis condition of 1070 °C and 400 torr, the quantity of the SnO network reached nearly one third in volume of the total products, which amounted to about 1 g for the small furnace we used. The reproducibility of the SnO network is good, and we can always obtain this kind of nanostructures inside the same region of the alumina tube under certain experiment parameters.

The as-synthesized material was characterized by scanning electron microscopy (SEM) (Hitachi S800 FEG), transmission electron microscopy (Hitachi HF-2000 FEG at 200 kV and JEOL 4000EX high-resolution TEM at 400 kV) and energy dispersive X-ray spectroscopy (EDS).

Received: March 6, 2002
Final version: April 5, 2002

[1] X. F. Duan, Y. Huang, J. F. Wang, C. M. Lieber, *Nature* **2001**, *409*, 66.
[2] Y. Cui, C. M. Lieber, *Science* **2001**, *291*, 851.
[3] M. H. Huang, S. Mao, H. Feick, H. Q. Yan, Y. Y. Wu, H. Kind, E. Weber, R. Russo, P. Yang, *Science* **2001**, *292*, 1897.
[4] M. T. Bjork, B. J. Ohlsson, T. Sass, A. I. Persson, C. Thelander, M. H. Magusson, K. Deppert, L. R. Wallenburg, L. Samuelson, *Appl. Phys. Lett.* **2002**, *80*, 1058.
[5] B. Mayers, Y. Xia, *Adv. Mater.* **2002**, *14*, 279.
[6] A. M. Morales, C. M. Lieber, *Science* **1998**, *279*, 208.
[7] S. T. Lee, N. Wang, Y. F. Zhang, Y. H. Tang, *MRS Bull.* **1999**, 36.
[8] D. P. Yu, Z. G. Bai, Y. Ding, Q. L. Hang, H. Z. Zhang, J. J. Wang, Y. H. Zou, W. Qian, G. C. Xiong, H. T. Zhou, S. Q. Feng, *Appl. Phys. Lett.* **1998**, *72*, 3458.
[9] Y. C. Choi, W. S. Kim, Y. S. Park, S. M. Lee, D. J. Bae, Y. H. Lee, G. S. Park, W. B. Choi, N. S. Lee, J. M. Kim, *Adv. Mater.* **2000**, *12*, 746.
[10] F. Krumeich, H. J. Muhr, M. Niederberger, F. Bieri, B. Schnyder, R. Nesper, *J. Am. Chem. Soc.* **1999**, *121*, 8324.
[11] M. Gao, S. M. Huang, L. M. Dai, G. G. Wallace, R. P. Gao, Z. L. Wang, *Angew. Chem. Int. Ed.* **2000**, *39*, 3664.
[12] J. Liu, et al., unpublished.
[13] See the articles in: *MRS Bull.*, August **2000**.
[14] Z. L. Wang, Z. C. Kang, *Functional and Smart Materials—Structural Evolution and Structure Analysis*, Plenum Press, New York **1998**.
[15] Z. W. Pan, Z. R. Dai, Z. L. Wang, *Science* **2001**, *291*, 1947.
[16] Z. R. Dai, Z. W. Pan, Z. L. Wang, *J. Phys. Chem. B* **2002**, *106*, 902.
[17] Z. W. Pan, Z. R. Dai, Z. L. Wang, *Appl. Phys. Lett.* **2001**, *80*, 309.
[18] Z. R. Dai, J. L. Gole, J. D. Stout, Z. L. Wang, *J. Phys. Chem. B* **2002**, *106*, 1274.
[19] Z. R. Dai, Z. W. Pan, Z. L. Wang, *J. Am. Chem. Soc.* **2002**, in press.
[20] Y. Q. Zhu, W. K. Hsu, W. Z. Zhou, M. Terrones, H. W. Kroto, D. R. M. Walton, *Chem. Phys. Lett.* **2001**, *347*, 337.

## White Light Emission Using Triplet Excimers in Electrophosphorescent Organic Light-Emitting Devices**

By *Brian W. D'Andrade*, *Jason Brooks*, *Vadim Adamovich*, *Mark E. Thompson*, and *Stephen R. Forrest**

A general solution to the problem of efficient white light generation in organic light-emitting devices is demonstrated using the novel process of phosphor excimer emission. These electrophosphorescent organic light-emitting devices solve the problem of interactions between multiple dopants for the generation of white light by using a single phosphor for blue emission, as well as for forming excimers that emit from green to red. Energy transfer between dopants (leading to current-dependent color changes) is significantly reduced since excimers lack a bound ground state, thus offering a simplified means to achieve broad spectral emission from organic light-emitting devices. This approach is well suited to low-cost white light emitters, which eventually might replace existing,

[*] Prof. S. R. Forrest, B. W. D'Andrade
Center for Photonics and Optoelectronic Materials (POEM)
Princeton Materials Institute (PMI)
Department of Electrical Engineering, Princeton University
Princeton, NJ 08544 (USA)
E-mail: forrest@ee.princeton.edu
J. Brooks, V. Adamovich, Prof. M. E. Thompson
Department of Chemistry, University of Southern California
Los Angeles, CA 90089 (USA)

[**] The authors thank Universal Display Corporation, the Defense Advanced Research Projects Agency, and the National Science Foundation's Materials Research Science and Engineering Center for their support.

  0935-9648/02/1508-1032 $ 17.50+.50/0 